Extreme Mechanics Letters 50 (2022) 101529

Contents lists available at ScienceDirect

Extreme Mechanics Letters

journal homepage: www.elsevier.com/locate/eml

Peeling in electroadhesion soft grippers

Vito Cacucciolo [a,b,*], Herbert Shea [a], Giuseppe Carbone [b]

[a] Soft Transducers Laboratory (LMTS), École polytechnique fédérale de Lausanne (EPFL), Rue de la Maladière 71b, CH-2000 Neuchâtel, Switzerland
[b] Department of Mechanics, Mathematics and Management (DMMM), Politecnico di Bari, via E. Orabona n. 4, 70125 Bari, Italy

ARTICLE INFO

Article history:
Received 21 August 2021
Received in revised form 20 October 2021
Accepted 25 October 2021
Available online 16 November 2021

Keywords:
Electroadhesion
Soft grippers
Peeling
Soft robotics

ABSTRACT

Electroadhesion endows robots with super-human abilities: mechanical geckoes that climb vertical walls and soft grippers that grasp the most delicate objects. Based on electrostatics, the adhesion forces are turned on and off by an electrical signal, promising extremely fast operation, from silent fully solid-state devices. Practical applications of electroadhesion have however been limited to date by two main challenges: (1) the adhesion forces can vary over 1000x by simply changing the angle between the electroadhesive tape and the object, (2) release is often slow due to residual adhesion when voltage is removed.

This paper describes a solution to both these issues by understanding and leveraging peeling in electroadhesion. We present simple models for peeling of electroadhesive tapes, predicting a change in peeling force from < 1 mN to over 1 N by changing the angle between the tape and the object from 90° to 0°. The models are in excellent agreement with our peeling experiments with 30 mm long, 20 mm wide, 300 μm thick electroadhesion tapes made of silicone rubber with carbon electrodes.

We demonstrate an electroadhesion soft gripper that uses motorized fingers to control the peeling angle, as a practical application of our peeling models. By moving the fingers to ensure a low peeling angle (0°) when grasping, the same gripper can successfully pick up from a 10 g cherry tomato (2.5 cm wide) to a 600 g Mango (9 cm wide). By then setting a high peeling angle (> 30°), the gripper reliably and rapidly (< 300 ms) releases those objects, despite residual adhesion.

Electroadhesion soft grippers have many advantages, including grasping without squeezing, silent operation, low power consumption (< 1 W) and low weight (1 g per soft finger). Understanding and modelling contact mechanics in electroadhesion devices was an essential missing step for practical applications of electroadhesion in robots and grippers. This paper sheds light on how peeling influences electroadhesion and provides practical tools to design and operate electroadhesion systems.

1. Introduction

Soft grippers using Electroadhesion (EA) grasp without squeezing, enabling the pick-and-place of even the most delicate objects without damaging them [1]. These grippers, however, show a change of over 1000 times in their grasping force depending on the grasping posture [2]. Our hypothesis is that the dominant factor for this variation of the grasping force is the peeling angle between the EA surface and the object. The variation of the peeling force with the peeling angle is well known for other kinds of adhesives, such as dry and chemical adhesives [3]. In this paper, we demonstrate that peeling models developed for dry/chemical adhesives can successfully describe EA with minor adaptations: replacing the surface energy due to Van der Waals forces or chemical bonds with the EA surface energy and, when the adhesive is pulled parallel to the object's surface (angle $\theta = 0$), accounting for EA frictional stresses τ_{EA} and for the two surfaces to keep contact during pulling (Fig. 1a-b).

Electroadhesion is one of the few types of adhesion that can be switched on and off electrically [4,5]. It leaves no chemical residues, works on both smooth and rough surfaces and keeps its adhesion strength over time. It finds applications in climbing robots [6,7], soft grippers [1,2,8–11] and haptics [12,13]. To date, research on modelling EA focused on electrical or tribo-electrical aspects, while the mechanical side has been mostly overlooked [14–19]. In a previous exploratory work [2], we reported how the grasping force of a soft gripper made of two EA fingers changes from 10 mN to over 15 N by changing only the object size and the relative position between the fingers and the object. This result highlighted the importance of the peeling angle in EA.

The pioneering and still widely used peeling models first proposed by Rivlin in 1944 [20] and further developed by Kendall in 1971 [21] and 1975 [22] describe how the pulling force on an

* Corresponding author at: Department of Mechanics, Mathematics and Management (DMMM), Politecnico di Bari, via E. Orabona n. 4, 70125 Bari, Italy.
E-mail address: vito.cacucciolo@poliba.it (V. Cacucciolo).

https://doi.org/10.1016/j.eml.2021.101529

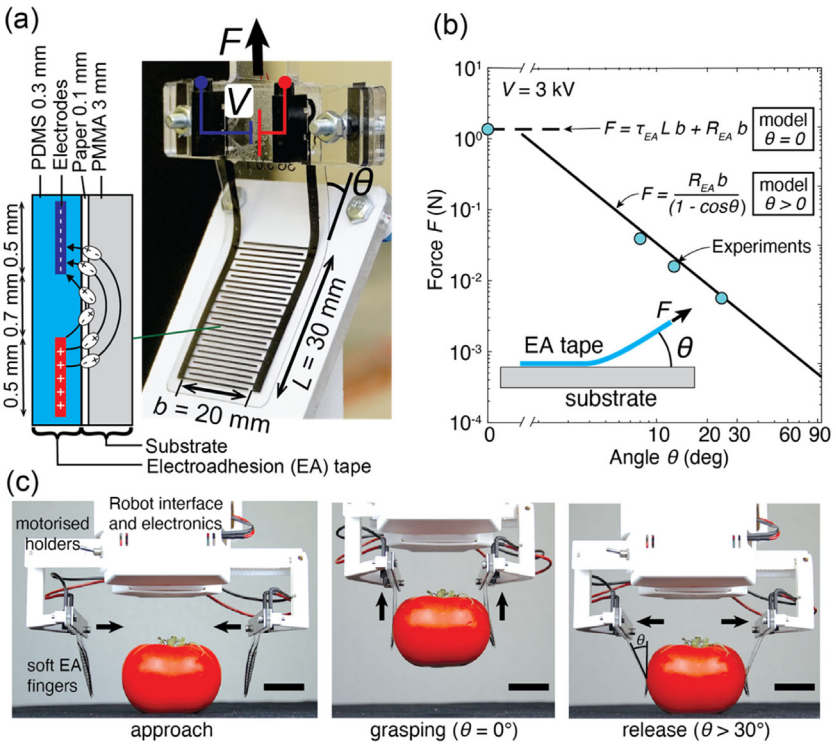

Fig. 1. Peeling of Electroadhesion (EA) tapes. (a) Schematic cross-section of the EA tape and photo of the characterization setup. (b) Plot of EA peeling force vs. peeling angles for the two models (solid and dashed lines) and experimental data (circles) presented in this work. (c) Our soft EA gripper uses low peeling angle (high force) for grasping, and large peeling angle (low force) for fast and reliable release. Scale bars 30 mm.

adhesive tape varies with the peeling angle, for both inextensible and elastic tapes. These models are based on crack propagation and do not include friction. The work of the pulling force is balanced by the energy required to create new surface at the crack tip. For relatively large values of the angle θ, the elastic energy can be neglected. For smaller θ ($<10°$), the forces become larger and the elastic energy in the tape becomes more important, as accounted by Kendall in 1975 [22]. Subsequent research extended these models by including friction, visco-elastic effects, and bending energy [3,23,24].

When $\theta = 0$ (lap shear configuration), the situation changes abruptly and additional parameters come into play, including frictional stresses, the compliance of the tape, its thickness and aspect ratio [25]. Most studies for lap shear configuration involve soft tapes with a stiff backing [26]. In this case, the failure mode is the entire tape suddenly detaching (rather than continuous unpeeling) when the pulling force exceeds a critical value [23]. The homogeneous distribution of the load over the whole area of the adhesive leads to very large detaching stresses (up to 30 N/cm^2 for dry adhesives) [27]. Such adhesives with stiff backing are generally bonded to flat surfaces. Soft grippers however must handle objects with complex shapes, often having non-zero gaussian curvature. For this reason, fully stretchable adhesives would be preferred for grippers. For stretchable tapes (no backing), two distinct failure modes have been reported, depending on the relative contribution of frictional stresses. When frictional stresses are low compared to adhesion energy, the failure mode resembles the one at low but finite peeling angles: a crack propagation front appears, and the pulling force reaches a steady value, proportional to the width of the adhesive and independent of its length [22,23]. When frictional stresses are dominant, a sliding region appears in which frictional stresses act. The sliding region grows during pulling, and the pulling force increases until reaching its critical value only when the sliding front reaches the end of the tape. The critical force in this case is proportional to the area of the adhesive. The frictional stress τ is uniform and steady in the zone of sliding [23]. The EA tapes studied in this letter when $\theta = 0$ exhibit the latter type of behaviour (homogeneous frictional stress τ acting over a sliding region whose length grows by increasing the pulling load).

This letter presents the first models and experimental characterization of peeling in EA (Fig. 1 a–b). We developed two models, one for $\theta > 0$ and one for $\theta = 0$, given the different physical parameters involved. When $\theta > 0$, the adhesion surface energy is the main parameter influencing the force required to detach the tape. Therefore, we based our model for $\theta > 0$ on Rivlin's model [20], for its simplicity and widespread use, where the only parameters involved are the (electro) adhesion surface energy and the peeling angle θ:

$$F = \frac{bR_{EA}}{1 - \cos\theta} \tag{1}$$

In this configuration, the force F required to detach the tape is proportional to the width of the tape b rather than to the area A, and it reaches a plateau for constant peeling angle θ.

When $\theta = 0$ (lap shear configuration), the adhesive is pulled parallel to the substrate and remains in contact with it during pulling. As reported in the literature for an elastomer tape with no rigid backing [23], we also observed that frictional stress τ plays a critical role, and that the force required to detach the tape is proportional to the area of adhesion A. The forces involved are much larger (>1 N) than in the $\theta > 0$ case.

The results from the presented models, confirmed by our experiments, show how the force required to detach an EA tape from a substrate changes orders of magnitude by changing the peeling angle (Fig. 1b). We demonstrate that a relatively simple adaptation of existing peeling models provides an accurate description of mechanics of EA, which can be used to design and operate EA soft grippers (Fig. 1c) and robots.

The paper is organized as follows. In Section 2 we present the experimental details. In Section 3 we report on the definition

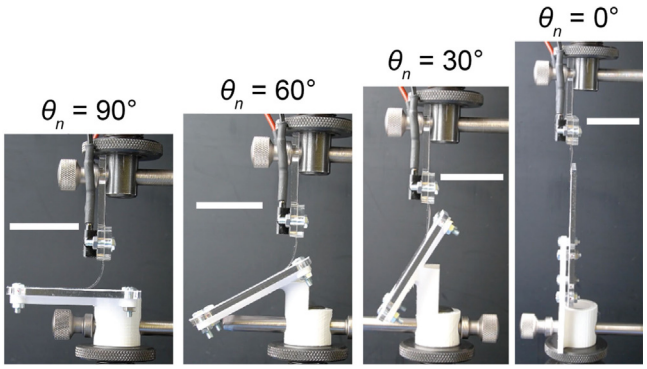

Fig. 2. Experimental set-up for the EA peeling test with the 4 nominal angles used. Scale bars 30 mm.

of the EA surface energy and the FEM (Finite Element Method) used for its numerical computation. Section 4.1 introduces the model for EA tapes when $\theta = 0$. This model includes frictional stress and considers the two surfaces remaining in contact during pulling. We present an experimental validation of the model. In Section 4.2 we describe our adaptation of Rivlin's peeling model for EA tapes by using the EA surface energy derived in Section 3. We report our peeling experiments for $\theta > 0$, and show that this model accurately predicts the force required to detach an EA tape. Section 5 presents a demonstration of how the understanding of peeling in EA can be used to design and operate a soft gripper, leveraging low peeling angles to generate large grasping forces and high angles for fast release. The gripper demonstrates grasping of a wide range of delicate objects. Finally, Section 6 draws the conclusions of this work, and proposes opportunities for future studies.

2. Materials and experimental methods

We conducted peeling tests by pulling an EA tape adhered to a fixed substrate, as shown in Fig. 2. The pulling direction was vertical. We used substrates with four different angles (θ_n) with respect to the pulling direction (0°, 30°, 60°, 90°). We measured force and displacement using an INSTRON 3340 Single Column Universal Testing System, moving at a speed of 0.1 mm/s and with a load cell with a 0.1 mN resolution and 50 N maximum load. The voltage was applied using a TREK 609E-6 power supply. We used a 1 Hz bipolar symmetric square wave at 0, 1, 2, and 3 kV. Pulling tests started 10 s after the voltage was applied and ended when reaching a displacement of 10 mm. We performed 3 trials for each combination of parameters.

In our loading condition, the angle θ between the tape and the substrate changes continuously during the test and differs from the nominal one θ_n imposed between the substrate and the pulling direction (Fig. 2). The variation of the peeling angle is a well-known and common condition in peeling tests. We recorded movies of each test and measured the actual angle θ from still frames (software: Kinovea).

The EA tapes were made of PDMS (Polydimethylsiloxane) with carbon-loaded PDMS electrodes. We used Sylgard 184 PDMS (Dow Corning) and Ketjenblack EC-300J carbon black (AkzoNobel). The geometry and architecture are shown in Fig. 1a. We fabricated the PDMS layers by blade-casting of liquid PDMS and the electrodes by blade-casting of the PDMS − carbon black slurry, followed by curing in the oven at 80° and laser ablation, to define the electrode geometry. The total thickness is $h = 290\ \mu m$. Thickness of electrodes is 30 μm. The distance between the electrodes and the surface in contact with the object is 60–80 μm. Given the low thickness and small area of the electrodes, we assumed for the EA tapes homogeneous material properties corresponding to those of PDMS Sylgard 184, namely a Young's modulus $E = 3.9$ MPa (16) in the linear elastic regime. The substrates are composed of a support structure made of 3D printed PLA (Polylactic Acid) and a plate made of laser-cut 3 mm-thick PMMA (Polymethyl methacrylate). We assumed the substrates as rigid given the ∼1000x higher Young's modulus of PLA (4 GPa) and PMMA (3 GPa) compared to PDMS. We covered the PMMA plates with paper (80 g/m^2) to minimize dry adhesion between the EA tape and the substrate.

3. Electroadhesion surface energy

We posit that the interaction between the EA tape and the substrate can be captured by two simple quantities: the EA frictional stress τ_{EA}, which will be treated in detail in Section 4.1, and EA surface energy R_{EA}. We define the EA surface energy as the variation in electrostatic energy stored in a capacitor formed by an electrode pair, when in contact with a substrate (capacitance C_{cont}) and when at infinite distance (capacitance C_∞), divided by the capacitor area

$$R_{EA} = \frac{1}{2}\frac{(C_{cont} - C_\infty)V^2}{A} \tag{2}$$

This model assumes that EA forces go to zero when the EA tape detaches from the surface and its validity is based on the knowledge that EA forces decay relatively fast with distance ($F \sim \frac{1}{d^2}$).

Given the coplanar geometry of our electrodes, the highly non-uniform electric field makes it unpractical to compute capacitance using analytical models. Therefore, we conducted FEM simulations using COMSOL Multiphysics to estimate C_∞ and C_{cont}. We set-up the simulations as 2-D in the cross-sectional plane (Fig. 3). The edges of the electrodes are rounded to avoid field singularities. We selected a set of equations corresponding to stationary electrostatics $\nabla \cdot \boldsymbol{D} = \rho_v$, $\boldsymbol{E} = -\nabla V$, with $\boldsymbol{D} = \varepsilon_0 \varepsilon_r \boldsymbol{E}$ the displacement field, $\boldsymbol{E}$ the electric field, ρ_v charge density, ε_0 vacuum permittivity and ε_r relative permittivity. The electrodes are modelled as contours with an applied constant potential difference V. Note that capacitance values are independent from the value of V. The different dielectric materials involved (PDMS, air, PMMA) have been accounted for through their relative permittivity ε_r (PDMS $\varepsilon_r = 2.7$ [28], air $\varepsilon_r = 1$, PMMA $\varepsilon_r = 3$). A relatively large bounding box on the top (3 mm) and bottom (4 mm) of the EA tape ensures that the electric field decays by over three orders of magnitudes at the boundaries compared to its value around the edge of the electrodes. Periodic boundary conditions on the sides allow using one semi-electrode pair to account for the entire EA tape. Once the geometry is fixed, C_∞ and C_{cont} are computed, corresponding to different values of the relative permittivity for the region on top of the EA tape: air ($\varepsilon_r = 1$) and PMMA ($\varepsilon_r = 3$). The electric field on one semi-pair of electrodes are shown in Fig. 3. Using an out-of-plane dimension $b = 20$ mm, the results give $C_{cont} = 0.41$ pF and $C_\infty = 0.29$ pF for a single semi-pair of electrodes (length 1.2 mm) and 10.3 pF at contact and 7.3 pF at infinity for the entire EA tape (length $L = 30$ mm). These values are comparable with measured capacitance in the literature for similar EA tapes [11]. Finally, the resulting EA surface energy computed as $R_{EA} = \frac{1}{2}\frac{(C_{cont} - C_\infty)V^2}{A}$ gives the results summarized in Table 1.

4. EA model and experiments at different peeling angle

4.1. EA peeling at $\boldsymbol{\theta} = 0$

This section presents a model for pulling an EA adhesive tape along a rigid substrate (Fig. 4a) in lap shear configuration, with

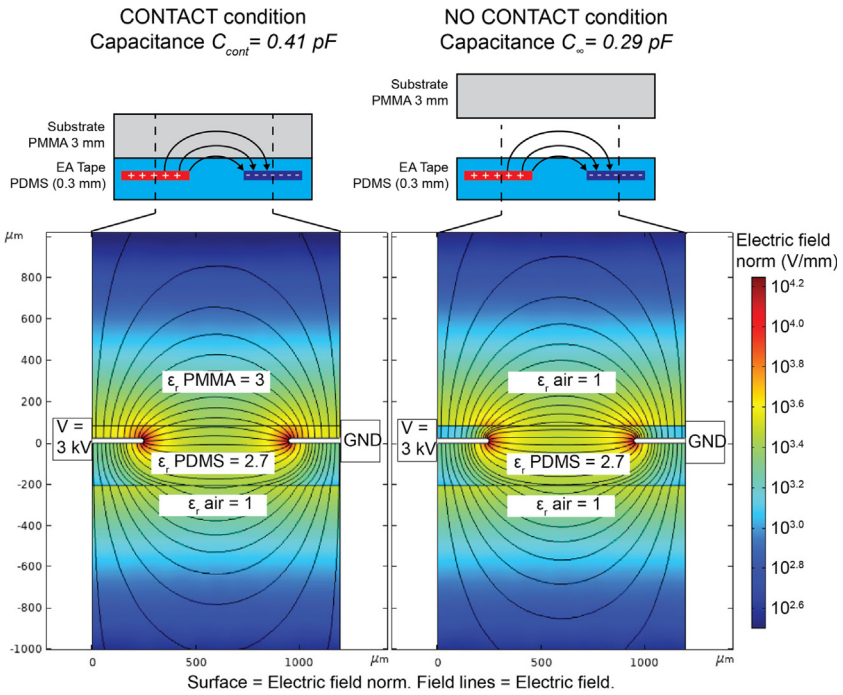

Fig. 3. FEM simulations of electric field used to compute the capacitance of a semi-electrode pair. (Left) in contact with the substrate (PMMA on top), (right) at infinite distance from the substrate. For simplicity, we neglected the 0.1 mm-thick copy paper layer.

Table 1
Electroadhesion surface energy R_{EA} at different values of applied voltage.

V (kV)	0	1	2	3
R_{EA} (J/m^2)	0	0.0025	0.010	0.023

the pulling force parallel to the surface of the substrate ($\theta = 0°$). Classical peeling models are based on crack propagation and assume a sliding front that propagates along the tape during the test [22,23]. This configuration does not match what we observed when pulling EA tapes, where the surface of the EA tape remains in contact with the substrate during the test. As described in the introduction, we observed for EA tapes in lap-shear mode the creation of a sliding region, whose length a increases with the pulling force F. The frictional stress τ_{EA} is uniform and constant over this region. When a reaches the length of the tape L, the pulling force reaches a critical load beyond which the entire tape slips releasing strain energy and then quickly re-adheres to the substrate. Stick–slip behaviour has been reported previously for elastomers adhered on glass plates [23], but a formal model had not been published. Our model includes frictional stress τ_{EA} applied over the sliding surface and surface forces due to the creation of new surface, at the edge of the substrate (Fig. 4a). The model assumes quasi-static equilibrium in each instant of time. The details of the derivation of the model and its validity conditions are reported in the Appendix.

During each instant of time, the pulling force F is balanced by the frictional stress τ_{EA} acting over the shear friction region $\tau_{EA} * ab$, plus the force due to the creation of new area at the edge of the substrate $R_{EA} * b$

$$F = \sigma^{+}bh = \tau_{EA}ab + R_{EA}b \tag{3}$$

Both τ_{EA} and R_{EA} depend on the applied voltage V, but do not depend on the pulling force F. Therefore, as the pulling force F increases, the length of the shear friction region a has to grow to maintain balance.

When $a = L$, the whole EA section of the tape is subject to frictional stress. The system reaches its critical-load condition, as a further increase in the pulling force F cannot be balanced anymore and leads to the slippage of the EA tape. We can write the equilibrium at the critical-load

$$F_{MAX} = \tau_{EA}Lb + R_{EA}b \tag{4}$$

The maximum load that the EA tape can hold, F_{MAX}, depends on the frictional stress τ_{EA} multiplied by total adhered area Lb plus the EA surface energy R_{EA} times the tape width b.

The measured critical forces at different applied voltages V are plotted in Fig. 4b.

We derived τ_{EA} from the critical-load condition, using measured values of critical forces: $\tau_{EA} = \frac{F}{db} - \frac{R_{EA}}{L}$, when $a = L = 30$ mm. Our data (Fig. 4c) show how the frictional stress induced by EA τ_{EA} increases with V^2, until reaching a value of 2.3 kPa at 3 kV. The values are consistent with shear pressure data in the literature for similar voltage and distance between the electrodes and the object (60–80 μm) [11]. The estimated electric field in the dielectric at 3 kV is ∼20 kV/mm (3 kV/ (2 × 70 μm), well below the estimated breakdown limit of ≥100 kV/mm for PDMS Sylgard 184 [29]. We limited our tests at 3 kV to reduce the chance of electrical breakdowns that could damage and degrade the samples, since the scope of this work is not to measure the maximum force that can be generated by EA tapes but rather to characterize peeling in EA. Higher forces and frictional stresses can be obtained at higher voltage, following the quadratic law shown in Fig. 4b–c. The dependence of τ_{EA} on V^2 aligns with the V^2 dependence of the Maxwell pressure generated between the electrodes and the substrate in normal direction. Such voltage-dependent frictional stress is consistent with the pressure-dependent frictional stress observed for elastomers in contact with rough surfaces, in contrast with pressure-independent frictional stress for elastomers in contact with smooth surfaces [30]. In our case, the EA tape is made of silicone elastomer and the substrate is covered with paper, in order to make it rough and minimize dry adhesion.

For our EA tapes we can observe that the contribution of the frictional stress is much larger than the one of the surface energy when $\theta = 0°$. For $V = 3$ kV, we have $\tau_{EA} * b * L = 2.3$ kPa $*$

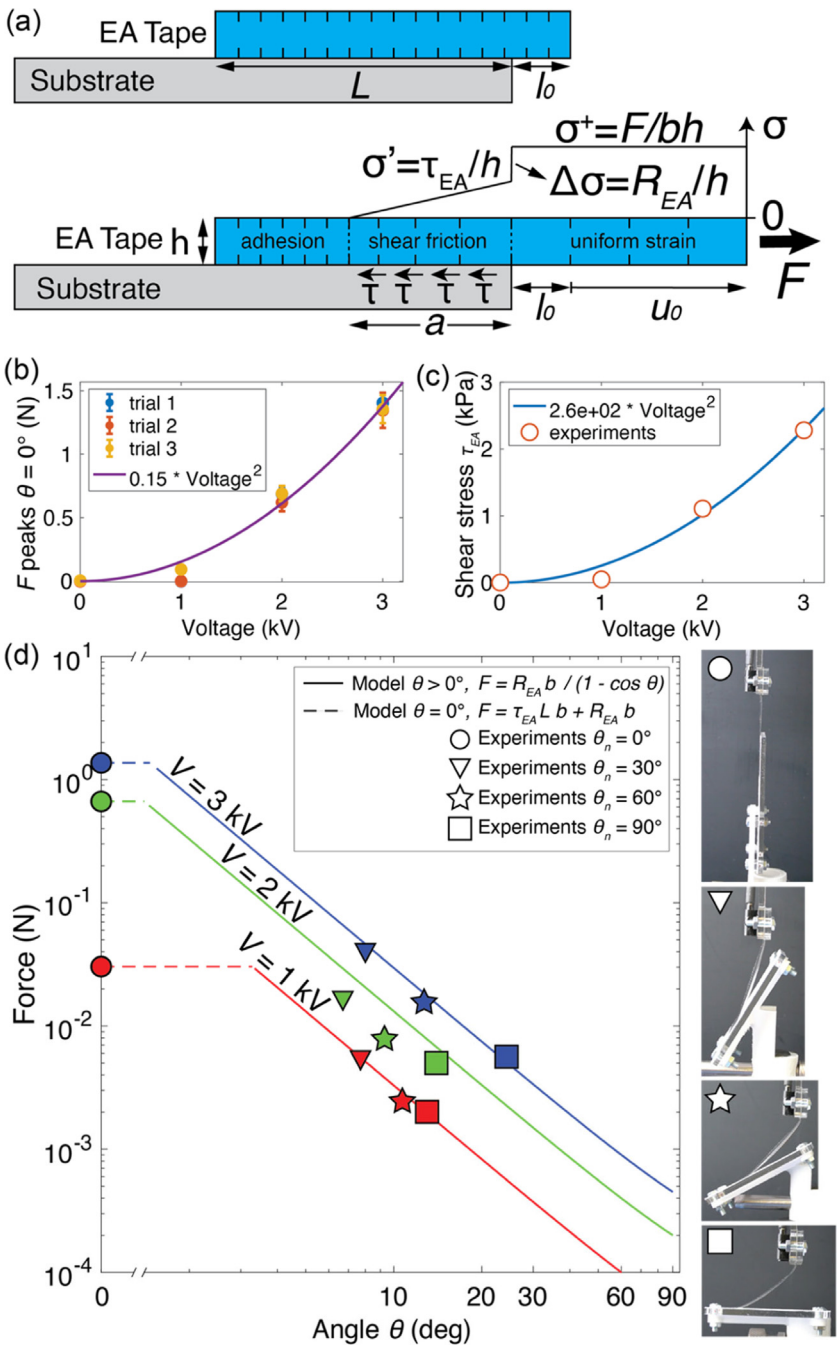

Fig. 4. Model results and experimental validation. (a-top) Pulling at $\theta = 0°$. EA tape adhered on a substrate, unloaded. (a-bottom) When loaded by the force F, the EA tape stretches and three distinct regions appear: adhesion region, where the tape does not move and the stress is zero; sliding region of length a (function of the load), where the tape is deformed and subject to the frictional stress τ_{EA}; uniform stress/uniform strain region of length $l = l_0 + u_0$ where the tape is subject to stress $\sigma^+ = F/bh$ (b is the width of the tape and h its thickness) and strain $\epsilon = \sigma^+/E$. The tape reaches the critical load, just before slipping, when $a = L = 30$ mm. (b) Measured force at slippage for different values of the applied voltage. (c) Frictional stress τ_{EA} at slippage, for different applied voltages. (d) Peeling force vs. peeling angle θ, for different applied voltages. We used one model for $\theta = 0°$ and one model for $\theta > 0°$. At $\theta = 0°$, the force is mostly balanced by shear friction τ_{EA} acting over the adhered area. At $\theta > 0°$ the work done by the peeling force is balanced by the energy required to create new surface, R_{EA}.

20 mm $*$ 30 mm $=$ 1.38 N and $R_{EA} * b = 0.023$ (J/m^2) $*$ 20 mm $=$ 0.46 mN.

The comparison between our model at critical-load and experimental data is shown in Fig. 4d. The force data at $\theta = 0°$ correspond to the average of the force peaks at slippage instants, extracted using a peak-finding algorithm. Figure S4 shows the raw data of the tests $\theta = 0°$ with highlighted the force peaks.

4.2. Electroadhesion peeling at $\theta > 0$

When $\theta > 0$, the pulling force removes the adhesive from the substrate, with the formation of a peeling front and the creation of new surface as the adhesive becomes separated from the substrate. The relatively low forces involved when $\theta > 0$ (10^{-3} to 10^{-1} N) lead to low EA tape deformation ($\ll$1% in our PDMS-based EA tapes). The contribution from frictional stress τ_{EA} becomes negligible and the work of the applied load is balanced

by the energy required for the creation of new surface. Therefore, in this case we adopted a simple and widely used peeling model [20,22], where we replaced the surface energy with the EA surface energy R_{EA}

$$F = \frac{bR_{EA}}{1-\cos\theta} \quad (1)$$

We defined the EA surface energy, R_{EA}, as the change in electrostatic energy from when the EA tape is in contact with the substrate to when it is at an infinite distance away (Section 3).

During our tests, the angle θ decreases while the force F increases. So, the actual angle θ between the EA tape and the substrate changes continuously during the test and differs from the nominal angle θ_n imposed between the substrate and the pulling direction (Fig. 2 and Video 1). For this reason, the values of angle θ shown for the data in Figs. 1b and 4c have been measured using image analysis from single frames extracted from videos of the tests.

As shown in figure S5, for $\theta_n = 30°$ and 60°, the load constantly increases during the test, until a critical load is reached and the EA tape detaches from the substrate (Video 1), with a sudden drop of the force. This behaviour is observed also for $\theta_n = 90°$ and $V = 1$ kV. In all these cases, we extracted the force value plotted in Figs. 1b and 4b from the test as the height of the drop in force when the tape detaches, and we measured from the videos of the tests the corresponding angle θ in the instant before detaching. For $\theta_n = 90°$ and $V = 2, 3$ kV, the tape does not fully detach until the end of the experiment (holder displacement = 10 mm), so we extracted the force value for Figs. 1b and 4b as the magnitude of the force at the end of the experiment and measured the corresponding angle θ. In this latter case, it became necessary to correct for the weight of the detached portion of the tape, so we subtracted its contribution as $F_w = \frac{1}{2}$ mg $= \frac{1}{2}\rho_{PDMS}\ Lb^*hg = 1.3$ mN, with $b^* = 30$ mm the width of the tape. As in our set-up the peeling angle changes during each test, we only extracted force–angle values for specific data points. We highlight that the criteria that we used for selecting the force–angle values to extract from the pulling tests are arbitrary and led by practical considerations. In theory, any force–angle value at any point in time during pulling tests is equally valuable, as long as at least a portion of the tape adheres to the substrate.

The comparison of the model with experimental data at different voltage values is summarized in Fig. 4d, showing very good agreement across the different angle values.

5. EA Soft gripper with controlled peeling angle

A highly promising application of Electroadhesion is in soft grippers for the pick and place of delicate objects, such as fruit and vegetables. EA soft grippers apply no normal forces on the object, minimizing the risk of damage and requiring no force sensors. The load-carrying ability of these grippers is strongly influenced by the grasping posture, due to peeling. Based on the fundamental understanding of peeling in EA and on the models presented in this work, we designed a soft gripper with controlled peeling angle (Fig. 5). The gripper has two trapezoidal fingers made of PDMS with carbon-loaded PDMS electrodes. The materials and overall geometry are inspired by previous works by the authors [1,2] and are aligned with the EA tapes tested in this letter, except for the trapezoidal shape. The width (from 45 to 10 mm) and length (45 mm) of the fingers are chosen to match common fruit and vegetables that can be picked by human hands. The trapezoidal shape allows picking up small objects such as cherry tomatoes using fingertips, while grasping large objects such as a 600 g Mango (Fig. 5) using the more proximal region of the fingers. The small thickness (0.3 mm) and soft materials used, let the gripper conform to the curvature of the object under EA forces.

We tested the gripper in the pick-and-place of delicate objects to demonstrate how controlling the peeling angle is essential to obtain successful grasping and release. The gripper is connected to a robot arm. The two EA fingers are mounted on motorized holders, whose distance can be adjusted from 0 to 90 mm using a servomotor and a rack-gear. This additional degree of freedom is what enables the control of the peeling angle between the fingers and the object. A successfully pick-and-place sequence is described as follows (Fig. 5a shows it for a 10 g cherry tomato and Fig. 5b for a 70 g lime): (1 approach) the fingers are positioned by the robot arm on the side of the object. (2 grasping) The fingers are closed by the motorized holders until they touch the object. The voltage is turned on. The robot arm moves vertically to pick the object (a roll rotation is added in Fig. 5a in to better display the shape of the gripper). A vertical movement of the robot with the fingers touching the surface of the object leads to a small peeling angle $\theta = 0°$ and a large grasping force. (3 release) The robot arm moves down to place the object on its new position. The fingers are opened by the motorized holders, creating a large peeling angle $\theta > 30°$, which leads to a fast and effective release of the object.

Fig. 5c, Video 2 and 3 show how an attempted grasping with large peeling angle ($\theta > 30°$) leads to a failure due to the low peeling forces. Fig. 5b, d and Video 3 show the successful grasping of a 70 g lime and a 600 g Mango.

Video 2 and 3 shows how attempted release with a small peeling angle $\theta = 0°$ leads to failure due to residual adhesion, even once the voltage is turned off. Residual adhesion is a known drawback of EA and is caused by both charge accumulation and dry adhesion resulting from the large Maxwell pressure. Using a large peeling angle is a highly effective method to overcome this drawback and obtain fast and reliable release with EA grippers.

EA generally requires high voltage (2–5 kV) to operate at the cm-scale. We powered our gripper demo using compact palm-sized power supplies, with very low currents (10 μA) and energy consumption (1 W). The low currents (intrinsically limited on the power board) ensure the safety for human operators even in case of accidental contact with a charged conductor. The low power consumption represents a significant advantage of EA grippers over pneumatic alternatives. An example of such compact high-voltage and low-current power supplies has been presented in a previous work by the authors [31].

6. Conclusions

In this paper, we demonstrate for the first time the influence of the peeling angle on the force required to detach a soft Electroadhesion (EA) tape. We presented two models, one for $\theta = 0°$ and one for $\theta > 0°$, due to the fundamentally different mechanisms governing these two cases. When $\theta = 0°$, the applied force $F_{MAX} = \tau_{EA}Lb + R_{EA}b$ is almost entirely balanced by the EA frictional stress created by the normal Maxwell stress, multiplied by the EA area $\tau_{EA} \times Lb$, while the contribution from the EA surface energy $R_{EA}b$ is negligible. In contrast, for $\theta > 0°$, shear stresses become negligible and the applied force is entirely balanced by EA surface energy $F = \frac{bR_{EA}}{1-\cos\theta}$. The developed models are compact and simple to use, yet show very good agreement with our experiments on the force required to detach the tape at different values of the angle θ.

Nonlinear effects such as necking of the tape when pulling at $\theta = 0°$ and hyperelastic material model for PDMS have not been included in this study and will be investigated in future work. Future investigations will also focus on the velocity-dependent forces, given the importance of visco-elastic effects in elastomers and the velocity dependence of frictional stresses [30].

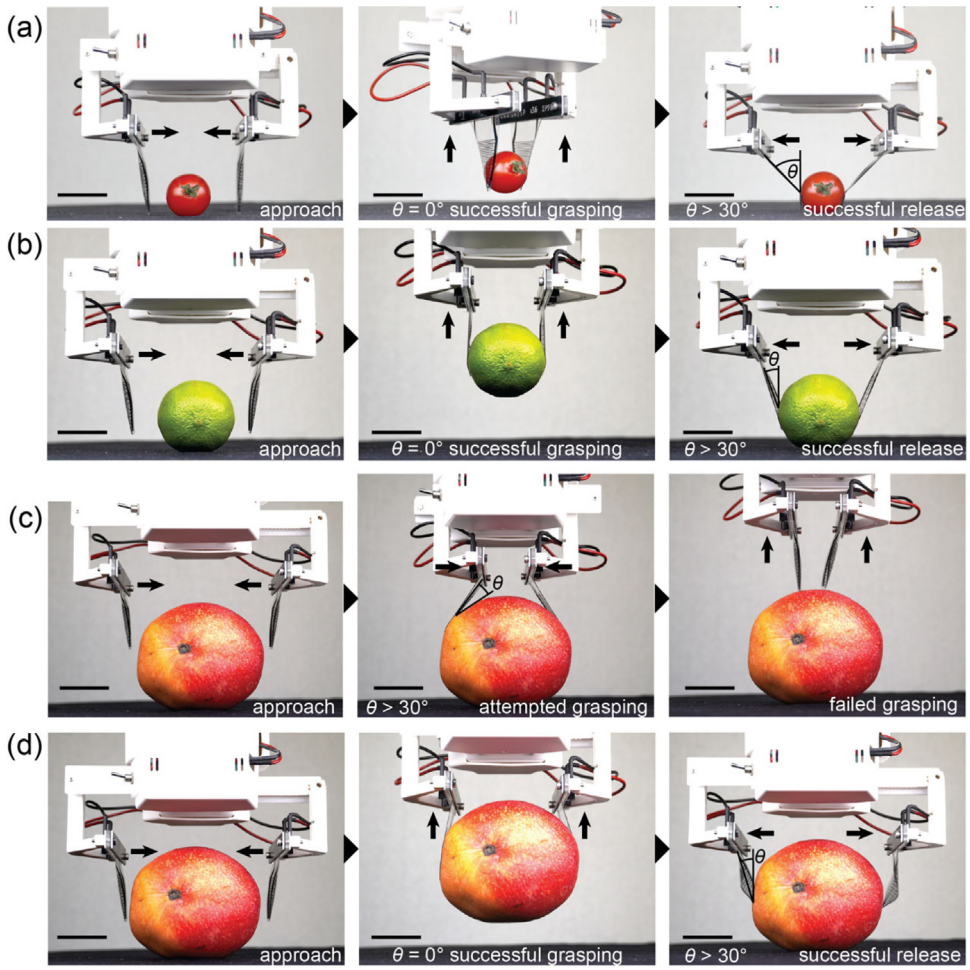

Fig. 5. Soft gripper using two EA fingers mounted on movable holders. The opening and closing of the holders, combined with the up–down movement of the robot arm, enables the gripper to grasp objects of different shapes and sizes. We adjust the peeling angle first to maximize the grasping force and then to minimize the adhesion force when releasing the object. (a) Successful grasping and release of a 25 mm wide cherry tomato (weight 10 g). (b) Successful grasping and release of a 50 mm wide lime (weight 70 g). (c) Demonstration of a failed grasping of a 90 mm wide mango (weight 600 g) with peeling angle >30°. (d) Successful grasping and release of a 90 mm wide mango (weight 600 g). Voltage 4 kV. Scale bar 30 mm.

This understanding of peeling effects in EA is essential for the design and operation of soft grippers and robots relying on EA. We demonstrated a dramatic dependence of EA forces with the peeling angle (>1000x) and provide simple model tools to design and operate EA systems. We presented a soft gripper that uses electroadhesion to pick and place a variety of delicate objects, such as fruit and vegetables. Previous EA grippers successfully grasped objects only in a narrow range of sizes, as the grasping forces quickly dropped due to peeling for larger and smaller objects. Another drawback of EA is the residual force when the voltage is turned off, which leads to slow release. Our gripper uses an extra degree of freedom (distance between the fingers) to control the peeling angle, which is used both for strong grasping on a wide range of object sizes and fast release by peeling off the fingers.

We demonstrated successful pick-and-place of a 600 g Mango (Fig. 5c and Video 3). The force values required to grasp this object (∼3 N/ finger) are larger than the pulling force measured in our tests on the EA tapes at 0° (Fig. 4d). The main reason for the higher force is arguably that the curvature of the Mango generates a further increase in frictional stress. This topic will be the subject of future study.

Electroadhesion has many advantages: low power consumption (<1 W), high forces (>15 N for 2 cm^2) and extremely compact form factors (∼100 μm thickness). We believe that this contribution will pave the way for the study of the mechanical and tribological aspects of electroadhesion, leading to a wider understanding of the underlying electro-mechanical phenomena and to the design of more advanced soft grippers, soft robots and wearables.

Declaration of competing interest

The authors declare the following financial interests/personal relationships which may be considered as potential competing interests: HS Electroadhesive device, system and method for gripping issued to Ecole Polytechnique Fédérale de Lausanne (EPFL), Lausanne (CH). VC Electroadhesion-based shear gripping system and method of using thereof pending to Ecole Polytechnique Fédérale de Lausanne (EPFL), Lausanne (CH). VC Electroadhesive gripping system and method for gripping an object pending to Ecole Polytechnique Fédérale de Lausanne (EPFL), Lausanne (CH). Two of the authors (V.C. and H.S.) are working on a project that could lead to the commercialization of a soft gripper technology.

Acknowledgements

We thank J. Shintake and R. Kanno (The University of Electro-Communications, Japan) for the discussion and feedback on Electroadhesion and V. Py (EPFL, Switzerland) for the technical support with the gripper demo.

This study was supported by the Swiss National Science Foundation and Innosuisse Bridge grant number 40B1-0_198680.

Appendix A. Supplementary data

Supplementary material related to this article can be found online at https://doi.org/10.1016/j.eml.2021.101529.

References

[1] J. Shintake, S. Rosset, B. Schubert, D. Floreano, H. Shea, Versatile soft grippers with intrinsic electroadhesion based on multifunctional polymer actuators, Adv. Mater. 28 (2) (2015) 231–238, http://dx.doi.org/10.1002/adma.201504264.

[2] V. Cacucciolo, J. Shintake, H. Shea, Delicate yet strong: Characterizing the electro-adhesion lifting force with a soft gripper, in: 2019 2nd IEEE International Conference on Soft Robotics (RoboSoft), 2019, pp. 108–113, http://dx.doi.org/10.1109/ROBOSOFT.2019.8722706.

[3] Z. Gu, S. Li, F. Zhang, S. Wang, Understanding surface adhesion in nature: A peeling model, Adv. Sci. 3 (7) (2016) 1500327, http://dx.doi.org/10.1002/advs.201500327.

[4] R.P. Krape, Applications Study of Electroadhesive Devices, 1968.

[5] A.B. Croll, N. Hosseini, M.D. Bartlett, Switchable adhesives for multifunctional interfaces, Adv. Mater. Technol. 4 (8) (2019) 1900193, http://dx.doi.org/10.1002/admt.201900193.

[6] H. Prahlad, R. Pelrine, S. Stanford, J. Marlow, R. Kornbluh, Electroadhesive robots—wall climbing robots enabled by a novel, robust, and electrically controllable adhesion technology, in: 2008 IEEE International Conference on Robotics and Automation, 2008, pp. 3028–3033, http://dx.doi.org/10.1109/ROBOT.2008.4543670.

[7] G. Gu, J. Zou, R. Zhao, X. Zhao, X. Zhu, Soft wall-climbing robots, Science Robotics 3 (25) (2018) http://dx.doi.org/10.1126/scirobotics.aat2874.

[8] G.J. Monkman, An analysis of astrictive prehension, Int. J. Robot. Res. 16 (1) (1997) 1–10, http://dx.doi.org/10.1177/027836499701600101.

[9] G. Monkman, Electroadhesive microgrippers, Ind. Robot 30 (4) (2003) 326–330, http://dx.doi.org/10.1108/01439910310479595.

[10] J. Shintake, V. Cacucciolo, D. Floreano, H. Shea, Soft robotic grippers, Adv. Mater. 30 (29) (2018) 1707035, http://dx.doi.org/10.1002/adma.201707035.

[11] N. Berdozzi, et al., Rapid fabrication of electro-adhesive devices with inkjet printed electrodes, IEEE Robot. Autom. Lett. 5 (2) (2020) 2770–2776, http://dx.doi.org/10.1109/LRA.2020.2972838.

[12] C.D. Shultz, M.A. Peshkin, J.E. Colgate, Surface haptics via electroadhesion: Expanding electrovibration with Johnsen and Rahbek, in: 2015 IEEE World Haptics Conference (WHC), 2015, pp. 57–62, http://dx.doi.org/10.1109/WHC.2015.7177691.

[13] M. Ayyildiz, M. Scaraggi, O. Sirin, C. Basdogan, B.N.J. Persson, Contact mechanics between the human finger and a touchscreen under electroadhesion, Proc. Natl. Acad. Sci. USA 115 (50) (2018) 12668–12673, http://dx.doi.org/10.1073/pnas.1811750115.

[14] D. Ruffatto, J. Shah, M. Spenko, Increasing the adhesion force of electrostatic adhesives using optimized electrode geometry and a novel manufacturing process, J. Electrost. 72 (2) (2014) 147–155, http://dx.doi.org/10.1016/j.elstat.2014.01.001.

[15] J. Guo, T. Bamber, M. Chamberlain, L. Justham, M. Jackson, Optimization and experimental verification of coplanar interdigital electroadhesives, J. Phys. D: Appl. Phys. 49 (41) (2016) 415304, http://dx.doi.org/10.1088/0022-3727/49/41/415304.

[16] S.B. Diller, S.H. Collins, C. Majidi, The effects of electroadhesive clutch design parameters on performance characteristics, J. Intell. Mater. Syst. Struct. 29 (19) (2018) 3804–3828, http://dx.doi.org/10.1177/1045389X18799474.

[17] J. Guo, J. Leng, J. Rossiter, Electroadhesion technologies for robotics: A comprehensive review, IEEE Trans. Robot. 36 (2) (2020) 313–327, http://dx.doi.org/10.1109/TRO.2019.2956869.

[18] J.D. West, J. Mici, J.F. Jaquith, H. Lipson, Design and optimization of millimeter-scale electroadhesive grippers, J. Phys. D: Appl. Phys. 53 (43) (2020) 435302, http://dx.doi.org/10.1088/1361-6463/aba1b0.

[19] B.N.J. Persson, General theory of electroadhesion, J. Phys.: Condens. Matter (2021) http://dx.doi.org/10.1088/1361-648X/abe797.

[20] R.S. Rivlin, The effective work of adhesion, Paint Technol. IX (106) (1944) http://dx.doi.org/10.1007/978-1-4612-2416-7_179.

[21] K. Kendall, The adhesion and surface energy of elastic solids, J. Phys. D: Appl. Phys. 4 (8) (1971) 1186–1195, http://dx.doi.org/10.1088/0022-3727/4/8/320.

[22] K. Kendall, Thin-film peeling-the elastic term, J. Phys. D: Appl. Phys. 8 (13) (1975) 1449–1452, http://dx.doi.org/10.1088/0022-3727/8/13/005.

[23] S. Ponce, J. Bico, B. Roman, Effect of friction on the peeling test at zero-degrees, Soft Matter 11 (48) (2015) 9281–9290, http://dx.doi.org/10.1039/C5SM01203A.

[24] N. Menga, L. Afferrante, N.M. Pugno, G. Carbone, The multiple V-shaped double peeling of elastic thin films from elastic soft substrates, J. Mech. Phys. Solids 113 (2018) 56–64, http://dx.doi.org/10.1016/j.jmps.2018.01.010.

[25] M.D. Bartlett, A.B. Croll, A.J. Crosby, Designing bio-inspired adhesives for shear loading: From simple structures to complex patterns, Adv. Funct. Mater. 22 (23) (2012) 4985–4992, http://dx.doi.org/10.1002/adfm.201201344.

[26] T. Yin, G. Zhang, S. Qu, Z. Suo, Peel of elastomers of various thicknesses and widths, Extreme Mech. Lett. 46 (2021) 101325, http://dx.doi.org/10.1016/j.eml.2021.101325.

[27] M.D. Bartlett, A.B. Croll, D.R. King, B.M. Paret, D.J. Irschick, A.J. Crosby, Looking beyond fibrillar features to scale gecko-like adhesion, Adv. Mater. 24 (8) (2012) 1078–1083, http://dx.doi.org/10.1002/adma.201104191.

[28] Sylgard 184 Technical Data Sheet. [Online]. Available: https://www.dow.com/content/dam/dcc/documents/en-us/productdatasheet/11/11-31/11-3184-sylgard-184-elastomer.pdf?iframe=true.

[29] F.B. Albuquerque, H. Shea, Influence of humidity, temperature and prestretch on the dielectric breakdown strength of silicone elastomer membranes for DEAs, Smart Mater. Struct. 29 (10) (2020) 105024, http://dx.doi.org/10.1088/1361-665X/aba5e3.

[30] M. Trejo, C. Fretigny, A. Chateauminois, Friction of viscoelastic elastomers with rough surfaces under torsional contact conditions, Phys. Rev. E 88 (5) (2013) 052401, http://dx.doi.org/10.1103/PhysRevE.88.052401.

[31] V. Cacucciolo, J. Shintake, Y. Kuwajima, S. Maeda, D. Floreano, H. Shea, Stretchable pumps for soft machines, Nature 572 (7770) (2019) 516–519, http://dx.doi.org/10.1038/s41586-019-1479-6.